Proceedings of ASME Turbo Expo 2011
GT2011
June 6-10, 2011, Vancouver, British Columbia, Canada

GT2011-46011

Effect of Narrow Jet Spacing on Impinging Flow and Heat Transfer

L. Guo, Y.Y. Yan, Y. Q. Zu,
Research Division of Energy and Sustainability, Faculty of Engineering,
University of Nottingham, NG7 2RD, UK
laxlg2@nottingham.ac.uk, yuying.yan@nottingham.ac.uk

ABSTRACT

Limited by the structures of the engineering components, sometimes the narrow gap impingement with limited jet-to-target spacing is required in the practical situations. In order to obtain an improved understanding upon the effects of narrow gap impingement on surface heat transfer and to fill gaps in the limited literatures, experiments of multi-jet impingement have been carried out using different jet-to-target distance (0.5D and 1D). Different configurations of jet-array are adopted and the transient thermochromic liquid crystal (TLC) is applied for the acquisition of the heat transfer data. Reynolds number of the jet flow ranges from 2.43×10^4 *to* 5.39×10^4*. It shows that the impingement using 90º attack angle with a jet-to-target distance of 0.5D leads to non-uniform distributions of the Nusselt number, especially for the upstream jet-region. According to the experimental results, the jets with the non-orthogonal attack angle and staggered array perform better than the normal ones. Under the same experimental conditions, the staggered jets with 75º attack angle can give higher average Nusselt numbers with fewer fluctuations in the jet region.*

INTRODUCTION

To achieve the maximum thermal efficiency, the inlet temperature of the gas turbine engine has been increased significantly in the past decades. In such a situation, various cooling methods have been developed to provide protections for the engine components. Among these methods, jet impingement has been testified capable to give an efficient heat transfer between the coolant and the target surfaces by means of the forced convection. Thus, it has been widely applied to the leading edge of the turbine blade. Performance of the jet impingement can be improved by optimizing the relative jet parameters. In order to achieve this, a large amount of studies have been performed to investigate the effects of different jet-schemes on the impinging performance. Following parameters are commonly considered when planning a certain jet-scheme, including the geometry of the nozzle, the attack angle, jet arrangement, jet-to-surface distance etc.

In the area of the experimental studies, impingement cooling from circular jets is investigated by Bouchez and Goldstein[1,2] et al., it shows that the heat transfer coefficient and effectiveness are independent of temperature difference between the jet and the targets. San[3] et al. conducted a measurement on local Nusselt numbers performed by a circular jet with 90º attack angle and 2.0 of *H/D*. Under the different Reynolds numbers, the correlations between the local Nusselt number and Reynolds number are purposed. In their further studies[4,5] impingement flow produced by the circular holes with staggered array was examined to understand the influences of different factors on the surface heat transfer, new correlations are purposed. The characters of the jet flow from the elliptic nozzles have been studied by Husain and Hussain [6-8]. The jet flow from the elliptic holes was compared with the flow from the circular holes. It shows that the elliptic jets can produce considerably greater entrainment and mixing than the circular or plane jets. According to the experimental results from Chiu, Jang and Yan[9], both impinging force and cross-flow can be increased by decreasing the jet-to-target distance from 4.5 to 1.5. And the increase in the impinging force showed relatively more significant than the increment of the cross-flow. Effects of impingement on non-flat surface were investigated by Kanokjaruvijit[10] et al., a target plate with staggered arrayed dimples were tested under different cross-flow conditions. Using the jet-to-target spacing of 2.0, the heat transfer performance of the dimpled plate was aggravated comparing to that of the flat plate. The effects of obliquely impinging air jets are investigated experimentally by O'Donovan and Murray[11], the influences of the naturally occurring vortices within the impinging flow on the near-wall heat transfer were reported. Florschuetz[12,13] et al. conducted an extensive study for different arrays of jets. Heat transfer correlations for the impingement methods have been extracted from their measurements. These correlations have been widely used in the industry design process.

Large amount of numerical studies were also carried out to investigate the jet impingement and heat transfer. According to Zuckerman[14] et al., the υ2f and SST models can provide better solutions for the flow properties of the impingement flow. Zu and Yan[15, 16]studied the capabilities of different turbulent models in predicting the jet impingement problems, the result shows that the SST model is most suitable when the computational cost and the accuracy are considered, correlations for the stagnation Nusselt number were presented. Numerical studies were carried out by Lou[17] et al. to examine the effects of geometric parameters on the confined impinging heat transfer. Effects such as the width of the nozzle, jet-to-target spacing, Reynolds number and roughness of the target plate are investigated.

Local heat transfer can be significantly influenced by the jet-to-target spacing, the *H/D*. Normally, the *H* value is always greater than the *D* value. But considering the actual situations through the turbine engine, sometimes the narrow gap impingement with limited jet-to-target spacing presents itself on certain occasions due to the structural constraint. Van Treuren[18] et al. found that the jet flow does not reaches a fully development only after a distance of approximately 6 hole-diameters from the jet exit. Thus, the narrow jet impingements with *H/D* values less than 1 are expected to give different cooling effects compared with the normal jets.

According to the literature survey in the current stage, a big amount of studies have been carried out upon the cooling effects of the jet impingements using $H/D \geq 1$. However, for the impingements with *H/D* value less than 0.5, few works can be tracked during the past two decades. Before it can be put into practical applications, detailed understandings in the mechanisms of these narrow-gap impingements have to be gained. The motivation of the present study is to understand the effects of these narrow gap impingements ($H/D \leq 0.5$) on surface heat transfer. Here, a couple of jet-to-target distances of 0.5*D* and 1*D* are applied and investigated experimentally using different jet schemes. The behaviours of the jet flow and the heat transfer results of the impingement are presented.

TEST FACILITIES AND DATA ACQUISITION

In present study, a test rig has been built for the application of transient thermochromic liquid crystal(TLC). Fig.1 gives the schematic view of the experiment system which consists of the airflow supply components, test control units, data acquisition units and the test section. The air is supplied by a 5.5kW blower whose speed can be controlled using a wall mounted inverter. A pipe mean velocity of the flow in a range of 3.1~ 20 m/s can be achieved. The flow then goes through a three element in-line duct heater which is controlled by a 15Amp variable AC power potentiometer unit. An ISO5167 standard orifice plate has been installed at the location of $20D_{duct}$ downstream the heater to obtain the mass flow rate through the pipe-work. During the test, the fluctuation of the flow temperature can be kept within ±0.5℃. This temperature is monitored by a four-wire resistance temperature detector (RTD) downstream of the orifice plate. The distance between the RTD and the orifice plate is $5D_{duct}$. Two pneumatic valves at the downstream of the heater are employed to control the air path during the experiment. Initially before the start of the each test, the hot air is expelled to outdoor atmosphere through a bypass duct to ensure the heated air is isolated from the test section. The response time of the valves have been initially tested and shows lower than 0.2s. Delay in the response time of the valve has been taken into account as one of the influencing factors of the experiment uncertainty. As the air exit the second pneumatic valve, it then approaches the impingement plate inside the test section. The properties of the air were calculated by ideal gas law using the reference temperature measured by the RTD.

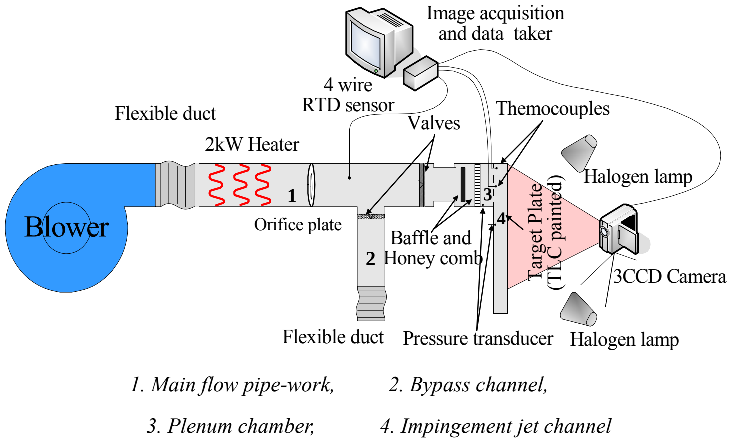

Fig. 1-Scheme of experimental facility setting up

The test section is manufactured by clear Perspex sheets with the thickness of 12 mm and designed to be able to easily dismount and replace from the end of the main pipe-work. The airflow firstly impacts onto a flow barrier used to distribute the flow into four parts and lead them to a downstream honeycomb straightener. Space between the flow straightener and the impingement plate is designed as a plenum chamber before the jets. Two pressure taps and a couple of K type thermocouples are located on the side walls of the plenum chamber normally to the flow direction before the jets. Another two pressure taps are disposed at 15D downstream the last row of jets to obtain the pressure information after the jets.

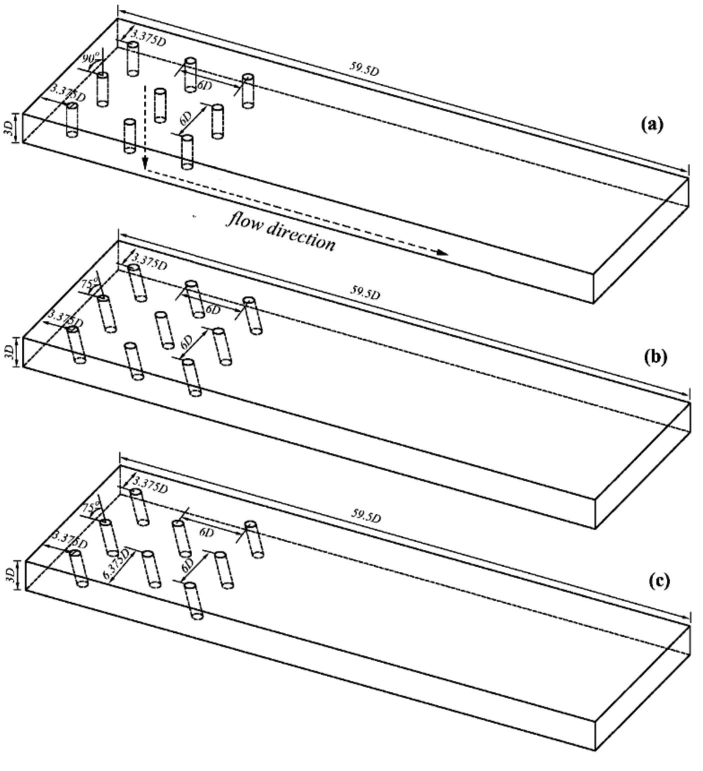

Fig.2-Geometry of Jet Plates

Three jet plates with different arrangements of the holes have been adopted, including one with 90° attack angle, and another two with 75º attack angle. For the two plates of 75º attack angle, the impingement holes are arranged in in-line array and staggered array respectively. The configurations of plates are shown in Fig.2.

The thermal images given by the TLC are captured by a 3CDD video camera situated in front of the target plate with a settled viewing angle of 90 degree. A pair of 300W tungsten halogen lamps has been fixed on both side of the target plate at where the reflection of light from the Perspex plate has been avoided. The lampshades have been simply modified with a double glazed shield was added. The radiative heating effect from the lamps thus can be eliminated by this water-floodable shield.

Black paint backed TLC (SPN/R38C5W, Hallcrest) with a temperature range from 35℃ to 49℃ is initially sprayed on the acrylic target plate. According to Wang, Ireland and Jones [19, 20] the value of hue depends on the ratio of RGB signals and shows normally increases monotonically with the temperature. A hue-analysis based data processing for application of the TLC has been widely accepted and therefore was employed in the present study. Since the calibration of the liquid crystal is vital for the identification of the hue value as well as the temperature determination, it has been performed in the current study using a method similar to Farina's[21]. The calibration bar is made of aluminium with a heater and a heat sink (ice-box) on both side of it. 8 *K*-type thermocouple probes were disposed equidistantly along its length. By this means the temperature distribution along the bar can be presented by both TLC and the thermocouples. The average value of the hue in spanwise direction was initially used to smooth the data, and then the hue–temperature relationship was re-averaged by a group of data obtained at different instants. Calibration results are shown in Fig.3, and the final correlation derived from the fitting curve is given by Eq.1.

$$T = 39.251 + 1.465 - ln\frac{0.47975}{0.65953 - H} - 1 \tag{1}$$

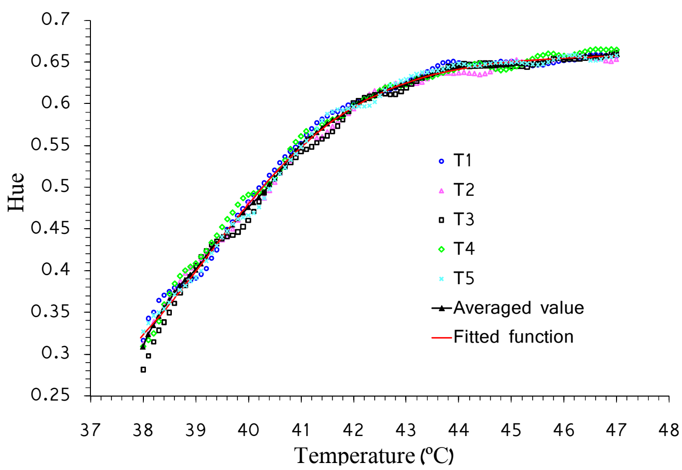

Fig. 3-Hue–Temperature Relationship and Fitted function

Investigation of accuracy showed that the maximum error between the calculated temperatures and test results is 0.11 ºC (less than 0.28%) for **H** ∈ [0.32, 0.6]

RESULT AND DISCUSSION

For the transient experiments, the heat transfer coefficient *h* was calculated based on the semi-infinite-plate solution. In the z-direction, *h* for the test surface can be obtained by solving

$$k\frac{\partial^2 T}{\partial z^2} = \rho C_p \frac{\partial T}{\partial t} \tag{2}$$

with the following initial and boundary conditions,

$$T(z,t)\big|_{t=0} = T_i \tag{3a}$$

$$-k\frac{\partial T(z,t)}{\partial z}\bigg|_{z=0} = h(T_w - T_m)\big|_{z=0} \tag{3b}$$

$$\lim_{z\to\infty} T(z,t) = T_i \tag{3c}$$

where T_w is the wall temperature; T_i is the initial surface temperature; T_m is the oncoming mainstream temperature. And ρ, C_p and k are density, specific heat and thermal conductivity of experimental material.

Using Duhamel's superposition theorem, the heat transfer coefficient can be represented as:

$$T_w - T_i = \sum_{j=1}^{n}\left\{1 - exp\left(\frac{h^2(t-\tau_j)}{\rho C_p k}\right)\cdot erfc\left(\frac{h\sqrt{(t-\tau_j)}}{\sqrt{\rho C_p k}}\right)\right\}\Delta T_{m(j,j-1)} \tag{4}$$

where, the $\Delta T_{m(j,j-1)}$ and τ_j are the temperature change of the flow and the time step, respectively. In the present study, $\Delta T_{m(j,j-1)}$ and τ_j were obtained by the thermocouples located at the exit of the jet orifice.

The uncertainties of the measured heat transfer coefficient were calculated using Eq.3 proposed by Moffat [22].

$$\frac{\partial \Theta}{\Theta} = \left\{\sum_{i=1}^{N}\left(\frac{\partial \Theta}{\partial X_i}\frac{\delta X_i}{\Theta}\right)^2\right\}^{1/2} \times 100\% \tag{5}$$

where, δX_i is the uncertainty of the independent variable. For the present study, δX_i for relevant parameters are given in Table.1.

Table 1-Uncertainties of the experimental parameters

Parameters, X_i	$\frac{\partial Nu}{\partial X_i}\frac{\delta X_i}{Nu}$
Diameter of the jets, D	±0.5%
Wall temperature (Initial), T_i	±2.5%
Wall temperature, T_w	±4.5%
Wall thermal diffusivity, Λ	±4.2%
Main stream temperature, T_m	±3.6%
Time, t	±0.4%

Calculations shows that for the Reynolds number of 2.4×10^4 ~5.4×10^4, the total uncertainty of the measured heat transfer coefficient for the present study is not more than 7.6%.

Four jet-configurations are presented in this paper. Considering the aim of the present study, three of them are configured using narrow jet-to-target spacing of H/D=0.5. The jet configurations and the operating conditions of the experiment are given by Table.2.

Table 2-Jet Configurations and Operating Conditions

α (°)	Array	*H/D*	Number of holes	*Re*
90	Inline	1.0	9	2.44×10^4;3.44×10^4 4.73×10^4;5.40×10^4
	Inline	0.5	9	2.34×10^4;3.16×10^4 4.73×10^4;5.37×10^4
75	Inline	0.5	9	2.29×10^4;3.22×10^4 4.67×10^4;5.21×10^4
	Staggered	0.5	8	2.40×10^4;3.30×10^4 4.85×10^4;5.30×10^4

Effect of the jet-to-target spacing

Effects of the jet-to-target spacing on surface heat transfer were studied using a couple of *H/D* values, the first one is 1.0 and the second one is 0.5. In-line array of nine single nozzles with 90° attack angle was adopted for both of the schemes.

Fig.4 shows the local Nusselt number distributions obtained using 1.0D jet spacing. In the present study, the Nusselt number is defined by

$$Nu = \frac{hD}{k(T_f)} \qquad (6)$$

where, the $k(T_f)$ is the thermal conductivity of the air evaluated at the mean film temperature $T_f=(T_w+T_a)/2$. T_w and T_a are the averaged temperature of the target plate and the air flow, respectively.

Note, in order to cut the computational cost, only 50% picture dots in spanwise direction were analysed during the post-processing. Results for the other half surface were obtained from data mirroring.

Here, a group of progressive Reynolds numbers in the range of 2.43×10^5 ~ 5.39×10^5 were employed for different cases. As shown in Fig.4, for cases of lower Reynolds number, the highest Nusselt numbers occurred at the stagnation points beneath each jet. While, for the case with highest Reynolds number (Fig.4-d), the peak values for the first row of the jets occurred in the circular regions around the stagnation points. This phenomenon is agreed with the experimental results obtained by Obot [23] et al. and Van Treuren [24] et al. And it is believed to be attributed to the jet interactions with the quiescent air near the edges of the jets. However, under the lower Reynolds number, the interactions between the jet flow and the channel air may be not aggressive enough to cause this highest heat transfer region around the stagnation points.

The valley values of the local Nusselt number appeared at the diamond region in the centre of the jet-squares composed of each four neighbour jets. The Nusselt numbers in the jet-region showed more sensitive to the change of the Reynolds number than those in the downstream region. After 17.5 of *x/D* location, the Nusselt numbers decreased quickly with the development of the flow towards the exit. When the Reynolds number increased from 2.43×10^4 to 5.91×10^4, the maximum enhancement in Nusselt number was more than 8 times for certain stagnation point in the upstream region, while only an enhancement of not more than 2 times was found for the downstream region. In addition, using the current confined one way model the development of the Nusselt number from the position underneath the jet to the exit of the channel exhibits a wavy characteristic. Moreover, it indicates that although increasing the jet Reynolds number shows effectively to increase the overall Nusselt number on the target plate, degradation in the uniformity of the flow structure and the heat transfer distribution occurs. More obvious phenomena can be found in the cases with *H/D*=0.5.

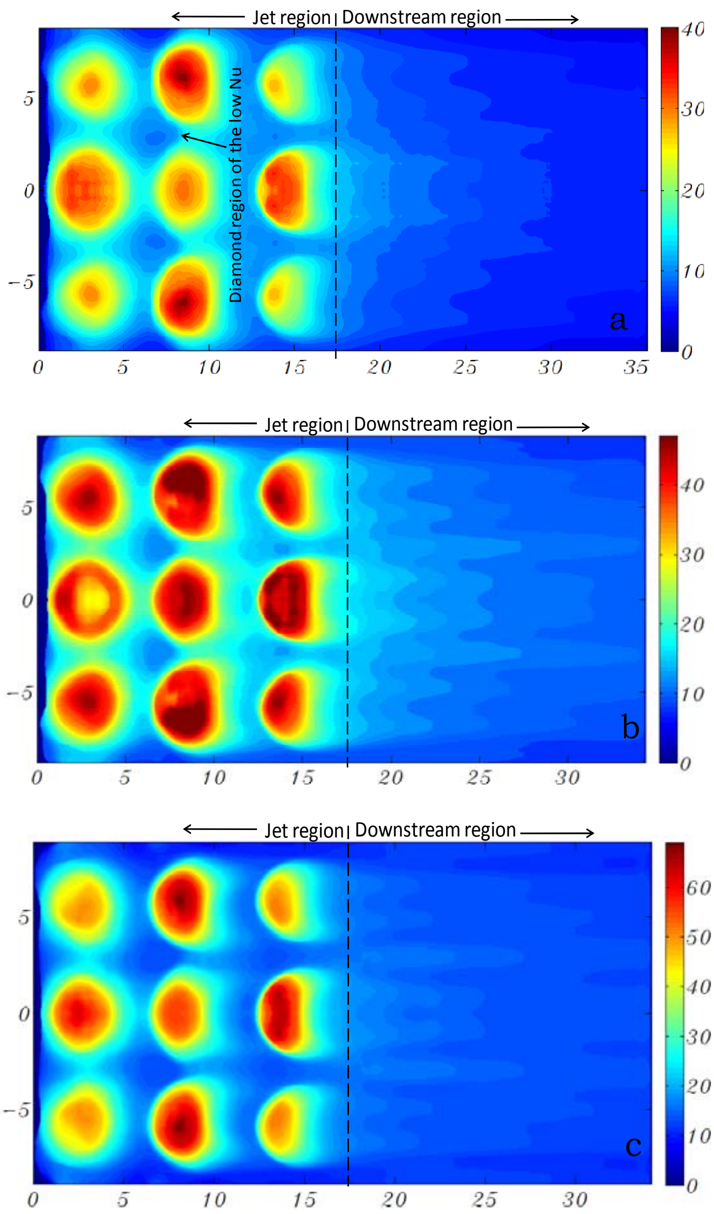

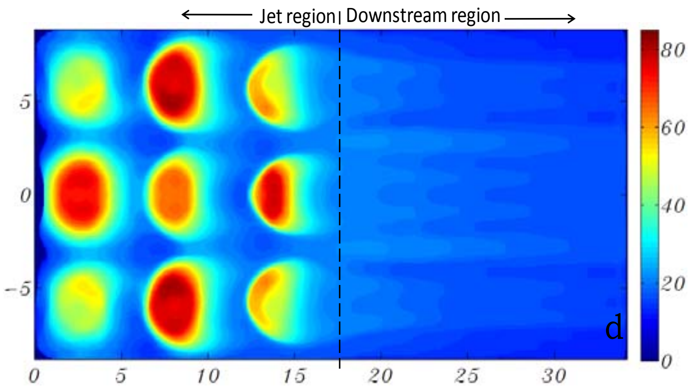

(a) Re_{jet} =2.44×10^4 (b) Re_{jet} =3.44×10^4
(c) Re_{jet} =4.73×10^4 (d) Re_{jet} =5.40×10^4

Fig.4-Nusselt number distributions over the target plate (In-line array, 90° attack angle, 1*D* spacing)

Results of the spanwise averaged Nusselt number of current study were compare with those obtained by Florschuetz et al.'s correlation[12,13] for *H/D*=1.0 of 90º in-line jets. (See Fig.5.) The correlation is written as,

$$\overline{Nu} = c\,Pr^{1/3}\,Re^{m}\left\{1-b\left[(H/D)(G_c/G_j)\right]^{n}\right\} \qquad (7)$$

for 2,500≤ Re≤ 70,000; 5≤ c_x/D ≤ 15(inline); 5≤ c_x/D ≤ 10 (staggered); 4≤ c_n/D ≤ 8; 1≤ H/D ≤ 3.

Where, *c, b, m,* and *n* are coefficients based on the jet characters, c_x and c_n are the streamwise and spanwise distances between holes; G_c is the cross-flow mass velocity based on channel cross sectional area, and G_j is the jet mass velocity based on jet hole area.

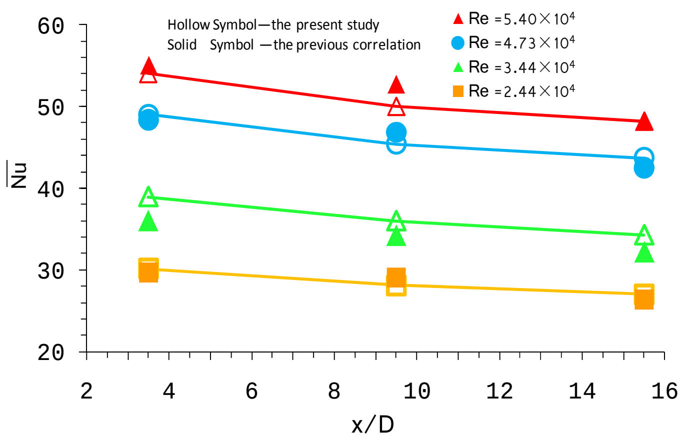

Fig.5-Comparison of spanwise averaged *Nu* with correlation

It shows the present results are in good agreement with the previous correlation. The maximum error between the test data and the results obtained from the correlation is not more 7.12%. The differences are within the total uncertainty of the measurement calculated by Eq.2. Since the correlation of Eq.7 is only validate for 1≤ *H/D* ≤ 3, therefore, no further comparison is carried out for the following results obtained using 0.5*D* jet spacing.

To understand the performance of the jet impingement using the extra narrow gap, 0.5*D* jet spacing was tested. Results are shown in Fig.6.

It is found that when a closer jet-to-target spacing was adopted, the patterns of the Nusselt number distributions upon the target plate turned more non-uniform. Although the stagnation points was still able to give the maximum Nusselt numbers over the whole plate, but for certain points, the magnitudes of the peak values seem lower than those shown in Fig.4. (e.g. the jets adjacent to the sidewalls in the first column). Meanwhile, it shows that with the application of the closer jet spacing, the areas of the high heat transfer region beneath the jets were reduced significantly. This indicates a further underdevelopment of the jet flow due to the reduced jet-to-target spacing. Downstream of the jet region from 16 of *x/D* location, two legs of the flow with higher Nusselt number can be observed developing towards the exit. A couple of low-heat transfer zones along the streamwise direction at spanwise locations of *y/D* =±3.5 can be seen at different Reynolds numbers. The above characters indicate that the reduced jet-to-target spacing will result in non-uniformed heat transfer distributions upon the surface and further lead to a lower area-averaged Nusselt number.

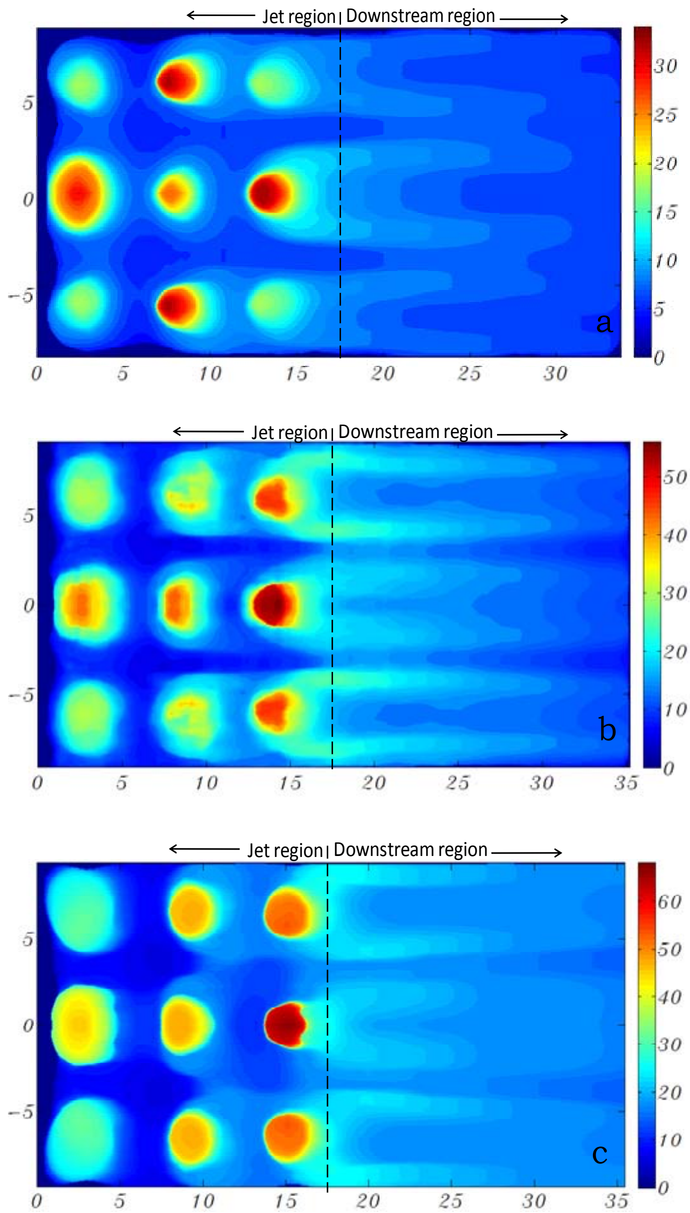

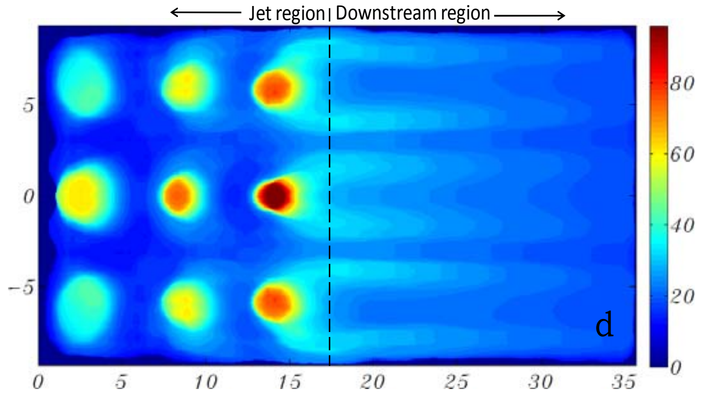

(a) $Re_{jet} = 2.34\times10^4$ (b) $Re_{jet} = 3.16\times10^4$
(c) $Re_{jet} = 4.73\times10^4$ (d) $Re_{jet} = 5.37\times10^4$

Fig.6-Nusselt number distribution over the target plate (In-line array, 90° attack angle, 0.5*D* spacing)

The area-averaged Nusselt number distributions for the cases using the normal jets are shown in Fig.7.

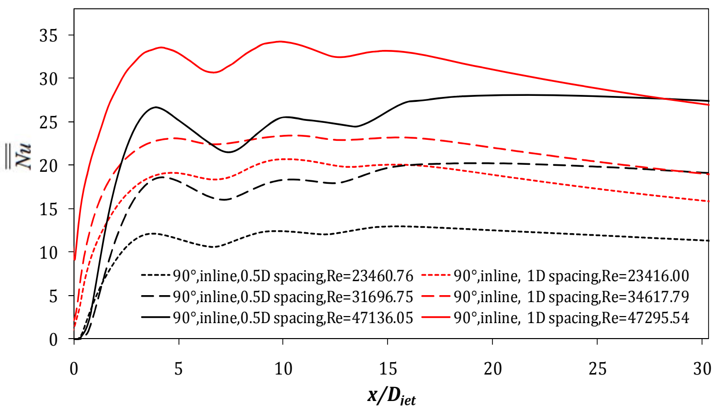

Fig. 7- Area-averaged *Nu* for in-line jets with 90° attack angle (Area-averaged along streamwise direction)

Using the in-line jets with 90º attack angle, the $\overline{\overline{Nu}}$ value decreases with the reduction of the jet-to-target spacing. Along the streamwise direction, in the region from 5 to 10 of *x/D*, notable fluctuations of $\overline{\overline{Nu}}$ can be found given by both of the jet-to-target distances. However, the fluctuations presented by the jets with 0.5*D* spacing look more obvious than that given by the other one. It indicates that with the application of the smaller jet-to-target spacing, the heat transfer distribution in streamwise direction tends to be more non-uniform, especially in the jet-region before the second column of the jets. The lowest $\overline{\overline{Nu}}$ in the jet region is found to occur at around 7.2 of *x/D* location. Another important contributing factor of the degraded heat transfer rates provided by the 0.5*D* spacing was thought to be the reduced discharge coefficients given by the closer spacing. Since the comparison of the C_d values shows that there was a reduction up to 3% in the discharge coefficient when the jet-to-target distance was reduced for 1*D* to 0.5*D*.

Effect of the attack angle and the arrangement of the jet-array

To obtain a comprehensive understanding of the performance of the narrow gap impingement used in the present study, the effects of the attack angle and the arrangement of the jet-array on heat transfer were investigated. A couple of jet arrangements with 75° attack angle are adopted, one is in-line array and another one is staggered array. Both of the configurations were applied with a jet-to-target spacing of 0.5*D*.

Fig.8 shows the Nusselt number distribution at four different Reynolds numbers given by the in-line array.

Compared with Fig.6, it finds that the peak value of the Nusselt number under the jets decreases with the attack angle, but the areas of the high heat transfer region beneath the impingement holes are enlarged by this inclined attack angle, particularly in the spanwise direction. It indicates that a higher diffusion rate of the jet flow may be achieved by using 75° attack angle. Moreover, better than the jets with 90° attack angle, the jets with 75° attack angle were found to give more uniform distributions of the Nusselt number downstream. Apparently, the two legs of the jet flow behind the cores of the last row showed by Fig.6 can no longer be seen in Fig.8

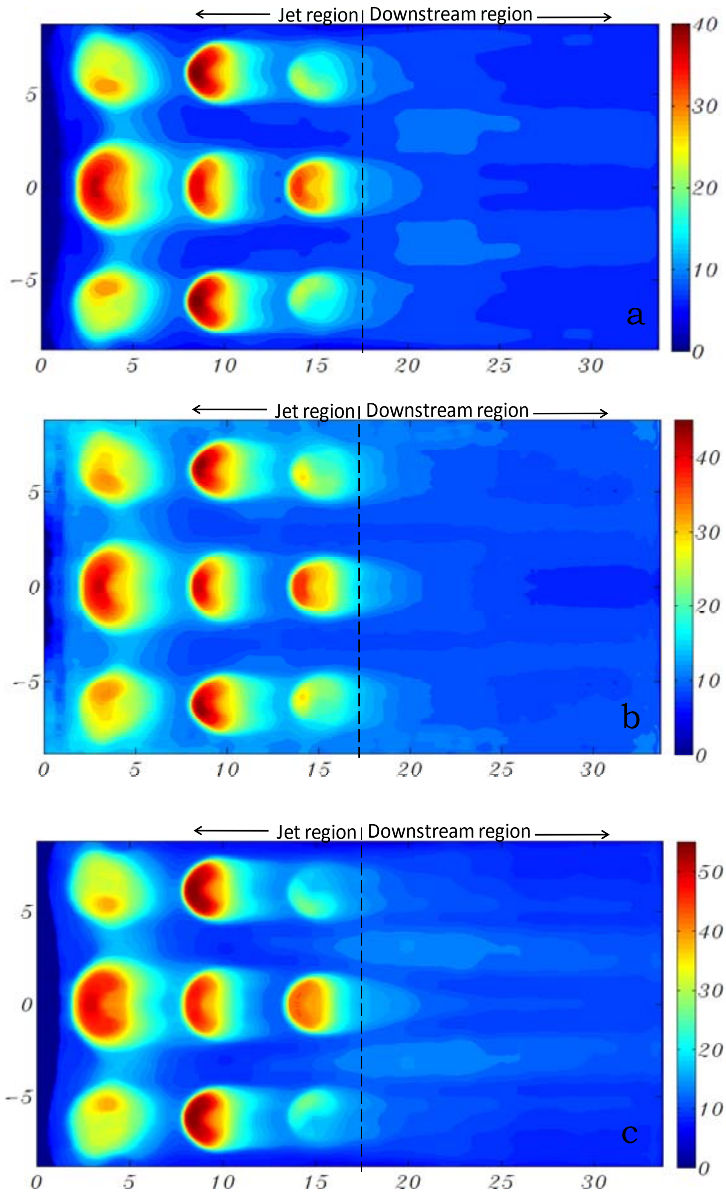

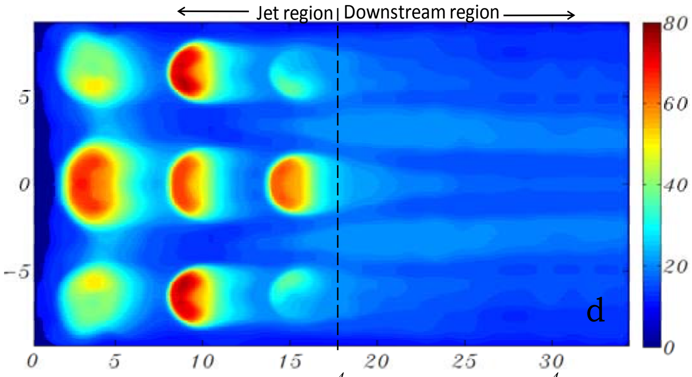

(a) $Re_{jet}=2.29\times10^4$ (b) $Re_{jet}=3.22\times10^4$
(c) $Re_{jet}=4.67\times10^4$ (d) $Re_{jet}=5.21\times10^4$

Fig.8- Nusselt number distribution over the target plate (In-line array, 75° attack angle, 0.5*D* spacing)

Patterns of the Nusselt number distributions obtained using the staggered jet-array with 75° attack angle are shown in Fig.9.

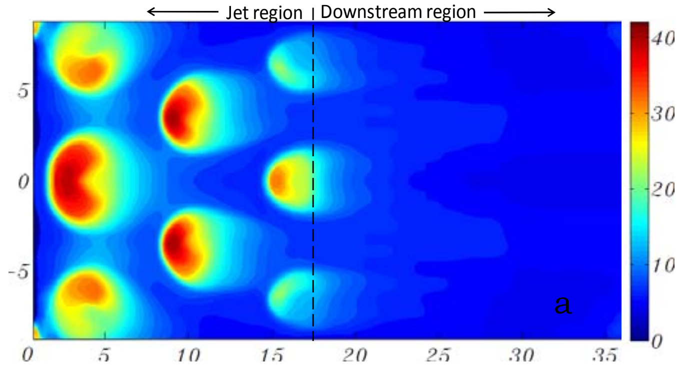

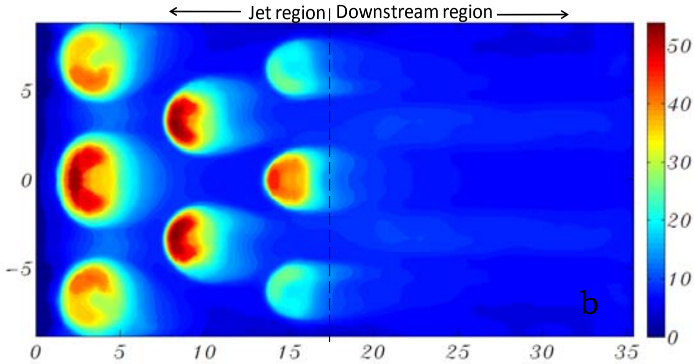

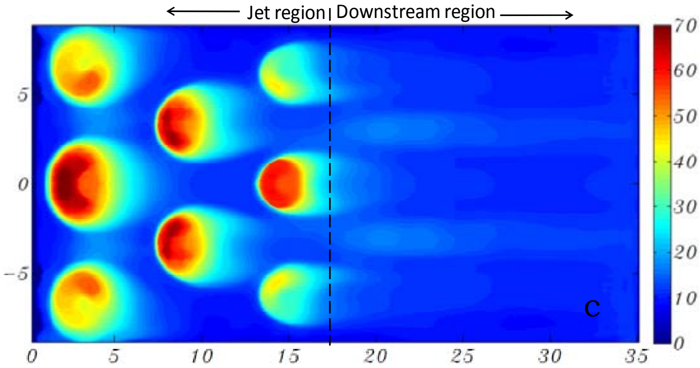

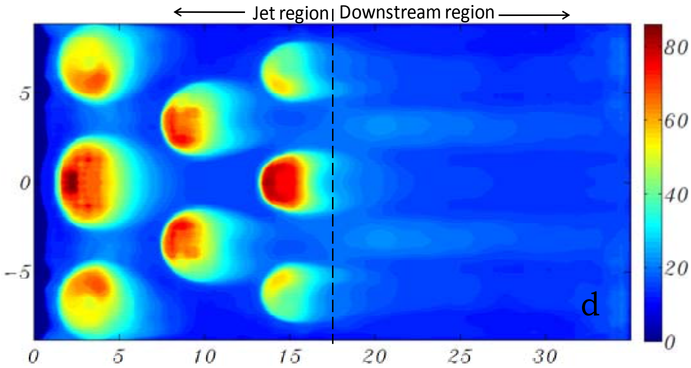

(a) $Re_{jet}=2.34\times10^4$ (b) $Re_{jet}=3.16\times10^4$
(c) $Re_{jet}=4.73\times10^4$ (d) $Re_{jet}=5.37\times10^4$

Fig.9-Nusselt number distribution over the target plate (Staggered array, 75° attack angle, 0.5*D* spacing)

It learns from the Fig.9, the structures of the jet flow presented by the staggered array are different to those given by the in-line array. Clearly, the shapes of the circular regions around the stagnation points were improved by using the staggered array, especially for the first two columns in the jet region. Since it was found that the lengths of the wakes behind the cores of the first and second columns were extended in streamwise direction when the staggered arrangement was adopted. This is because less jet-to-jet interactions can be achieved when the staggered array is adopted. Moreover, besides the circular regions beneath the jets, the wake-region always present higher Nusselt number than other regions. Thus, without the obstacle of the jet flow to the upstream cross-flow, the stagger array is able to promote the area-averaged Nusselt number in the jet region.

For the above two schemes of 75° attack angle, the influences of the jet arrangements on the area-averaged Nusselt number can be seen in Fig.10.

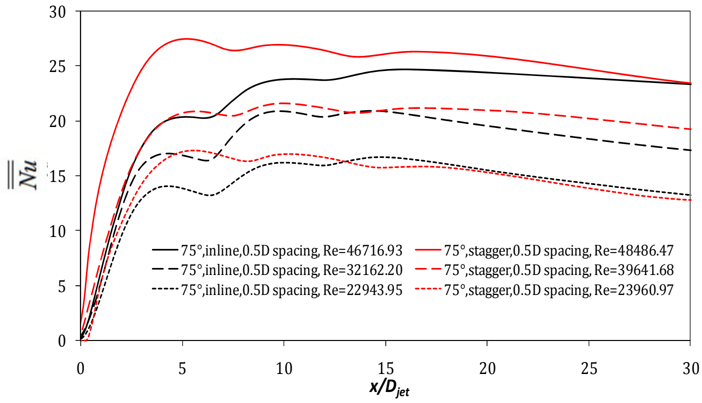

Fig.10-Area-averaged *Nu* for in-line and staggered jet-arrays (0.5*D* spacing, area-averaged along streamwise direction)

Fig.10 shows that under the same Reynolds numbers, the staggered array gave better area-averaged Nusselt for the jet region. The Nusselt numbers were boosted notably for the streamwise region from 0 to 15 of x/D when the staggered array was applied. The peak value of the area-averaged Nusselt number of using the stagger array appeared at the location of x/D=5 which was found occurred earlier than the peak value of the in-line array at 15 of x/D. It illustrates again that the staggered array can give more uniform Nusselt number distributions for the upstream region due to the fewer interactions between the jets. Moreover, note there are only 8 impingement holes have been employed for the staggered scheme which is less than the in-line scheme of 9 jets, thus a total mass flow rate in a lower level can be achieved by using the staggered one.

Further comparison between Fig.7 and Fig.10 shows that without changing the jet-scheme of the in-line array, the averaged Nusselt number in the jet region can be improved slightly by reducing the attack angle from 90° to 75°. Among the 3 jet schemes with 0.5*D* jet spacing, the staggered array with 75° attack angle provided the highest heat transfer rate for the jet region, meanwhile, less fluctuations along the streamwise direction. However, it shows that the jets using 90° attack angle was more capable in keeping a high Nusselt number after the jet region, thus it can be recommended for the situation in which the downstream heat transfer is important.

CONCLUSIONS

Experimental studies have been carried out to investigate the behaviour of the jet flow and heat transfer of a narrow gap impingement system. Circular jets in the form of in-line and staggered arrays with and 90 º and 75 º attack angles were employed in the present study. Totally, two *H/D* values of 0.5, 1.0 were tested under various Reynolds number ranged from 2.34×10^4 to 5.54×10^4. The major conclusion can be drawn as follow:

The increased Reynolds number is favourable to the local heat transfer over the target plate. Smaller *H/D* (0.5) is beneficial for the enhancement of the local Nusselt number over the stagnation points, but with the reduction of the *H/D* value, the area-averaged Nusselt number in the streamwise direction is found to be decreased significantly. Meanwhile, using the in-line jets with 90 º attack angle, the smaller jet-to-target spacing (0.5*D*) causes non-uniform distributions of the heat transfer, especially in the jet region. Hence, a lower area-averaged Nusselt number for the upstream surface. However, the 90º jets are found capable of keeping a higher $\overline{\overline{Nu}}$ for the downstream region. Without changing the in-line array, the $\overline{\overline{Nu}}$ can be improved slightly by reducing the attack angle from 90 º to 75 º.

Among the three jet-schemes of using 0.5*D* jet distance, the staggered array with 75 º attack angle gives a highest $\overline{\overline{Nu}}$ for the upstream jet region and less fluctuations for the whole surface, thus it is recommended for the further application.

ACKNOWLEDGEMENT

The authors wish to acknowledge the financial support from Siemens Industrial Turbomachinery Ltd, UK.

NOMENCLATURE

c_x	streamwise distance between the holes
c_n	spanwise distance between the holes
C_p	thermal capacity of the material
D_{duct}	duct diameter (m)
D	jet diameter (m)
G_c	cross-flow mass velocity
G_j	jet mass velocity based on jet hole area.
h	convective heat transfer coefficient (W/m^{2}K)
H	jet-to-target spacing (m)
k	thermal conductivity of the air (W/m K)
Nu	local Nusselt number
$\overline{Nu}$	spanwise averaged Nusselt number
$\overline{\overline{Nu}}$	surface averaged Nusselt number
Re_{jet}	jet-diameter based Reynolds number
t	time(s)
T_a	temperature of the air flow
T_i	initial temperature (K)
T_f	temperature of the air film upon the wall
T_w	local wall temperature (K)
ΔT_m	temperature change of the jet flow
δX_i	uncertainties of variables
τ	time step of the temperature change
x	*x*-coordinate (m)
y	*y*-coordinate (m)
ρ	density (kg/m^3)
Θ	experimental result

REFERENCE

[1]Bouchez, J.P. and R.J. Goldstein, *Impingement cooling from a circular jet in a cross flow.* International Journal of Heat and Mass Transfer, 1975. **18**(6): p. 719-730.

[2]Goldstein, R.J. and W.S. Seol, *Heat transfer to a row of impinging circular air jets including the effect of entrainment.* International Journal of Heat and Mass Transfer, 1991. **34**(8): p. 2133-2147.

[3]San, J.-Y. and M.-D. Lai, *Optimum jet-to-jet spacing of heat transfer for staggered arrays of impinging air jets.* International Journal of Heat and Mass Transfer, 2001. **44**(21): p. 3997-4007.

[4]San, J.-Y. and W.-Z. Shiao, *Effects of jet plate size and plate spacing on the stagnation Nusselt number for a* confined *circular air jet impinging on a flat surface.* International Journal of Heat and Mass Transfer, 2006. **49**(19-20): p. 3477-3486.

[5]San, J.-Y., Y.-M. Tsou, and Z.-C. Chen, *Impingement heat* transfer *of staggered arrays of air jets confined in a channel.* International Journal of Heat and Mass Transfer, 2007. **50**(19-20): p. 3718-3727.

[6]Husain, H.S. and F. Hussain, *Elliptic jets. Part 3. Dynamics of preferred mode coherent structure.* Journal of Fluid Mechanics, 1993. **248**: p. 315-361.

[7]Hussain, F. and H.S. Husain, *Elliptic jets. Part 1.* Characteristics *of unexcited and excited jets.* Journal of Fluid Mechanics, 1989. **208**: p. 257-320.

[8]Husain, H.S. and F. Hussain, *Elliptic jets. Part 2.Dynamics of coherent structures : pairing.* Journal of Fluid Mechanics, 1991. **233**: p. 439-482.

[9]Chiu, H.-C., J.-H. Jang, and W.-M. Yan, *Experimental study on the heat transfer under impinging elliptic jet array along a film hole surface using liquid crystal thermograph.* International Journal of Heat and Mass Transfer, 2009. **52**(19-20): p. 4435-4448.
[10]Kanokjaruvijit, K. and R.F. Martinez-botas, *Jet impingement on a dimpled surface with different crossflow schemes.* International Journal of Heat and Mass Transfer, 2005. **48**(1): p. 161-170.
[11]O'Donovan, T.S. and D.B. Murray, *Fluctuating fluid flow and heat transfer of an obliquely impinging air jet* International Journal of Heat and Mass Transfer, 2008. **51**(25-26): p. 6169-6179
[12] L. W. Florschuetz, C. R. Truman, and D. E. Metzger. S*treamwise Flow and Heat Transfer Distributions for Jet Array Impingement with Crossflow.* Journal of Heat Transfer 1981. **103**(2). p. 337-342.
[13] L.W. Florschuetz, D.E. Metzger, et al, *Jet array impingement with crossflow-correlation of streamwise resolved flow and heat transfer distributions,* NASA Contract Rep (1981).
[14]Zuckerman, N. and N. Lior, *Impingement Heat Transfer:* Correlations *and Numerical Modeling.* Journal of Heat Transfer, 2005. **127**: p. 544-552.
[15]Zu, Y.Q. and Y.Y. Yan, *Numerical Study on Stagnation Point Heat Transfer by Jet Impingement in a Confined Narrow Gap.* J. Heat Transfer 2009. **131**(9).
[16]Zu, Y.Q. and Y.Y. Yan. *CFD PREDICTION FOR* MULTI-*JET IMPINGEMENT HEAT TRANSFER*. in *ASME Turbo Expo 2009*. 2009. Orlando, Florida, USA.
[17]Lou, Z.Q., A.S. Mujumdar, and C. Yap, *Effects of* geometric *parameters on confined impinging jet heat transfer.* Applied Thermal Engineering, 2005. **25**(17-18): p. 2687-2697.
[18] Van Treuren, K.W., Wang, Z., Ireland, P.T., and Jones, T.V. *Detailed Measurements of Local Heat Transfer Coefficient and Adiabatic Wall Temperature Beneath an Array of Impinging Jets.* Journal of Turbomachinery. 1994.116: pp. 369-374.
[19]Wang, Z., P.T. Ireland, and T.V. Jones, *An advanced* method *of processing liquid crystal video signals from transient heat transfer experiments.* Jounal of Turbomachinery 1995. **117**: p. 184-189.
[20]Ireland, P.T. and T.V. Jones, *Liquid crystal* measurements *of heat transfer and surface shear stress.* Measurement Science and Technology, 2000. **11**: p. 969-986.
[21]Farina, D.J., et al., *Illuminant invariant calibration of* thermochromic *liquid crystals* Experimental Thermal and Fluid Science, 1994. **9**(1): p. 1-12.
[22]Moffat, Robert J. *Describing the uncertainties in experimental results.* Experimental Thermal and Fluid Science, 1988. **1**: p. 3-17.
[23]Obot, N.T., Majumdar, A.S., Douglas, W.J.M. *The Effect of Nozzle Geometry on Impingement Heat Transfer Under a Round Turbulent Jet.* 1979. ASME paper 79-WA/HT-53.
[24] Van Treuren, K.W., Wang, Z., Ireland, P., Jones, T.V., and Kohler, S.T. *The Role of the Impingement Plate in Array Heat Transfer.* 1996. ASME Paper 96-GT-162.

